Chemical Engineering Journal 497 (2024) 154610

Contents lists available at ScienceDirect

Chemical Engineering Journal

journal homepage: www.elsevier.com/locate/cej

Plastics adsorption and removal by 2D ultrathin iron oxide nanodiscs: From micro to nano

Yitong Cao [a], C.I. Sathish [a,*], Zhixuan Li [a], Muhammad Ibrar Ahmed [a], Vibin Perumalsamy [a], Chaojie Cao [a], Chenxi Yu [a], Binodhya Wijerathne [b], Adrew Fleming [c], Liang Qiao [d], Shaobin Wang [e], Jiabao Yi [a,*]

[a] Global Innovative Center of Advanced Nanomaterials, School of Engineering, University of Newcastle, Callaghan 2308, NSW, Australia
[b] School of Chemistry and Physics, Faculty of Science, Queensland University of Technology, Brisbane QLD 4000, Australia
[c] School of Engineering, University of Newcastle, Callaghan 2308, NSW, Australia
[d] School of Physics, University of Electronic Science and Technology of China, Chengdu, PR China
[e] School of Chemical Engineering, The University of Adelaide, Adelaide, SA 5005, Australia

ARTICLE INFO

Keywords:
Microplastics
Magnetic nanomaterials
Magnetic separation
Plastic pollution

ABSTRACT

The escalation of microplastics/nanoplastics (MPs/NPs) contamination in aqueous systems has ignited considerable concern. Magnetic separation has emerged as a promising remedy for the removal of these pollutants, owing to its notable removal efficiency, cost-effectiveness, and environmentally friendly attributes. This study presents the utilization of ultra-thin magnetic Fe_3O_4 nanodiscs (NDs) for the adsorption and separation of MPs/NPs. Investigations revealed that these NDs could effectively adsorb/remove MPs/NPs across a spectrum ranging from micro- to nano-scale, exhibiting a notable adsorption capacity of 188.4 mg g^{-1}. Mechanistically, MPs/NPs adsorption was driven by both electrostatic and magnetic forces originating from the vortex domain of NDs, which can be well described by pseudo-first-order and Sips models. Furthermore, the NDs exhibited outstanding reusability, maintaining over 90 % removal efficiency even after undergoing five cycles. This research introduces a cost-effective method for the separation of MPs/NPs, representing a significant stride in wastewater treatment methodologies.

1. Introduction

In the 21st century, the dependence of humans on plastics or plastic products has resulted in the large-scale production and extensive utilization of plastics, which has also intensified the mass spread of plastic waste and pollution [1]. According to statistical findings, a cumulative 6,300 million metric tons of plastic waste has been generated from the 1950 s to 2015, whereas merely 10 % of the produced plastic waste possesses the capacity for recyclability [2,3]. Plastic waste may be degraded by mechanical force, weathering, and microorganisms, thereby fragmenting into small debris referred to as microplastics (MPs) and nanoplastics (NPs) [4–6]. The term "microplastics," initially introduced by R. Thompson et al. in 2004, pertains to plastic fragments with a diameter of less than 5 mm [7,8]. The generated MPs may progressively amass in soil [9,10], sediment [11,12], and river [13], ultimately finding their way into the ocean [14]. The hazards associated with microplastics can be attributed to the following factors: (1) the leaching of toxic monomers and additives, (2) the release of the deleterious volatile organic compounds; (3) adsorbing persistent organic pollutants [15]. With the accrual of MPs within the ecosystem, MP pollution presents an underlying threat to terrestrial and marine ecosystems [16–18] and human health [19,20]. In instances of the widespread presence of MPs in the ecosystem, the removal and decomposition of MPs become a major global concern. Accordingly, a comprehensive exploration and development of methods and strategies to mitigate microplastic pollution are warranted.

In recent years, MP separation methods from an aqueous environment have been extensively developed, including filtration [21], froth separation [22], oil separation [23], magnetic separation [24], etc. Magnetic separation has attracted special attention due to its low cost, non-toxicity, and high efficiency. The principle underlying magnetic separation primarily hinges on the hydrophobic nature of MPs and the

* Corresponding authors.
E-mail addresses: sathish.ci@newcastle.edu.au (C.I. Sathish), jiabao.yi@newcastle.edu.au (J. Yi).

https://doi.org/10.1016/j.cej.2024.154610
Received 27 May 2024; Received in revised form 1 August 2024; Accepted 5 August 2024
Available online 6 August 2024

subsequent magnetizing of MPs, enabling them binding with magnetic materials. The movement of magnetized MPs can be influenced by magnets or an applied magnetic field, facilitating their facile removal from wastewater. In such cases, magnetic materials with strong hydrophobicity were applied for the magnetic separation of MPs. For an example, Fe nanoparticles hydrophobized by hexadecyltrimethoxysilane through surface modification could effectively adhere to the surface of MPs and magnetize them thereafter. This methodology attained excellent removal efficiency of 96 % and 88 % for polyethylene (PE) and polystyrene (PS) MPs (particle size < 20 μm), respectively, which were dissolved in artificial seawater [24]. Likewise, magnetite (Fe_3O_4) particles were used to separate polymethylmethacrylate (PMMA) and polyvinylchloride (PVC) MPs in pure water, yielding an approximate removal efficiency of 95 % within an optimal pH range [25]. Shi *et al* also used 30 nm of Fe_3O_4 nanoparticles to magnetize MPs and separate them from aqueous matrices by a magnet. For the PE, polypropylene (PP), PS and polyethylene terephthalate (PET) with a size of 200 nm, the optimal removal efficiency could reach 98 % [26]. Based on the surface modification with long-chain compounds, Wang et al. used Fe_3O_4 nanoparticles coated with fatty acid to obtain an adsorption efficiency of 92.89 % and an exceptional PS adsorption capacity of 809.29 mg g^{-1} [27]. For the surface functionalized magnetic nanoparticles and composites, the fabrication methods are complex and time-consuming. Moreover, these organic functional groups or composite components may leach into the aqueous environment during magnetic separation, leading to secondary contamination and the plastic pollutant exists in both nano and micro sizes. In addition to the magnetic nanoparticles, some magnetic adsorbents were also applied to MPs adsorption and removal. For instance, composites incorporating fly ash modified with Fe were synthesized to efficiently remove PS NPs while demonstrating a notable adsorption capacity (83.1 mg g^{-1}) [28]. Magnetic biochar has been extensively used to remove organic pollutants and MPs in wastewater due to the advantages of porous structure and low cost [29–31]. Likewise, N. Singh et al. used magnetic biochar composite to remove NPs by utilizing its high surface area [32]. However, the removal efficiency significantly decreased after utilizing the composite for five cycles. In practical wastewater, the active sites might be permanently filled by pollutants affecting the removal efficiency [33]. Hence, it is imperative to advance magnetic adsorbents to facilitate the facile adsorption and removal of plastic pollutant from both micro and nano scale with excellent reusability.

Magnetic ferrite nanodiscs (NDs) possess a special vortex domain magnetic state, [34] having the attributes of environmental friendliness, low cost and low toxicity. Therefore, magnetic nanostructures with vortex domain magnetic states have been widely used for magnetic resonance imaging [35,36], magnetic hyperthermia [37], bacteria detection [38], electrocatalysis [39] and wastewater treatment [40].

In this work, we synthesized 2D ultra-thin magnetic NDs using a hydrothermal method for adsorbing and separating MPs/NPs in an aquatic environment. These NDs have demonstrated remarkable adsorption capabilities of plastics pollutant from micro- to nano-scales with a high efficiency and reusability. The primary emphasis of the investigation is centred on the adsorption kinetics and isothermal analysis of the 100 nm NPs. The examination of adsorption interactions and processes were carried out utilizing scanning electron microscopy (SEM), photoluminescence (PL) spectrometry, and Fourier-transform infrared (FTIR) spectroscopy. In addition, the mechanism of magnetic separation and the contribution of magnetic materials exhibiting diverse magnetic states to the adsorption of magnetic particles were deliberated. The findings may furnish a novel theoretical reference for subsequent investigations into the removal of MPs.

2. Experimental procedures

2.1. Materials and chemicals

Iron (III) nitrate nonahydrate ($Fe_2(NO_3)_3{\cdot}9H_2O$), aluminium chloride ($AlCl_3$), and triethylamine (TEA) were purchased from Sigma-Aldrich. Polyamide (PA), PE, PP, PET, PS, PMMA, and PVC MPs were purchased from Mingyuexing Plastic Technology Co., Ltd., China. 100 nm of PS microbead suspension was purchased from Sigma-Aldrich. All the chemicals were used without further purification. Deionized (DI) water was sourced from the material science laboratory of University of Newcastle and the seawater was sourced from the Newcastle Beach, Australia.

2.2. Synthesis of iron oxide NDs

Iron oxide (α-Fe_2O_3) NDs were prepared hydrothermally by dissolving 0.647 g $Fe_2(NO_3)_3{\cdot}9H_2O$ and 0.08 g $AlCl_3$ in 16 ml DI water and stirring for 30 min. 4.6 ml of triethanolamine was then added to this mixture dropwise, and the stirring was continued for another 20 min. The well-mixed solution was sealed to a PPL (polyphenyl)-lined stainless-steel autoclave and treated at 160 ℃ for 24 h. The autoclave was cooled to room temperature, and the samples were collected and separated by centrifugation at 4500 rpm, then washed with DI water and ethanol for 5 times, and the final product was dried in vacuum at 80 ℃ overnight.

The Fe_3O_4 NDs were prepared by annealing α-Fe_2O_3 NDs in a tube furnace at 400 ℃, under a constant flow (100 sccm) of 5 % H_2 in argon for 5 h where the heating rate was maintained at 5 ℃/min. After annealing, the sample was cooled to room temperature and remained at this temperature for 5 h before being removed from the furnace.

2.3. Material characterization

The morphologies of iron oxide NDs and different kinds of MP nanostructures were examined by JEOL FE 7900F SEM. The crystal structure of Fe_3O_4 was investigated by JEOL F200 transmission electron microscope (TEM) at 200 kV voltage. Powder X-ray diffraction (XRD) patterns were measured by Bragg-Brentano geometric PANalytical Empyrean platform with a 0.1° fixed divergence slit and GaliPIX^{3D} multi-pixel detector. The XRD patterns were obtained by CuKα radiation source ($\lambda = 1.541$ Å) at 40 kV and 40 mA with a scan rate of 0.002°/sec from 10 to 80°. The specific surface area of NDs was determined by Brunauer-Emmett-Teller (BET) method and pore volume was measured at relative pressure (p/p_0) = 0.99. Magnetic properties were investigated by a superconducting quantum interference device (SQUID, Quantum design-PPMS). The thickness of NDs was measured by atomic force microscope (AFM) (NTEGRA II). The fluorescence spectra were recorded with a Perkin Elmer LS55 Luminescence spectrophotometer. The functional groups of NDs and MPs were determined by Fourier transform infrared spectra, obtained with a Perkin Elmer Frontier FTIR/NIR spectrometer using the KBr disk method. X-ray photoelectron spectroscopy (XPS) analysis was carried out using the multiprobe photoelectron spectrometer from Omicron Nanotechnology. Peak fitting and atomic concentrations were carried out using the Avantage software.

2.4. Preliminary MP separation experiments

Two types of MPs, i.e. PMMA and PS, in three different sizes (10 μm, 500 nm, and 100 nm) were used for investigating the adsorption capacity of NDs. 60 mg L^{-1} of MPs and 5 mg NDs were dispersed in 15 ml DI water and sonicated for 20 min. The MP suspension after sonication was incubated in an orbital shaker at 180 rpm at room temperature for 6 h. Then, the magnetized MPs were separated from the suspension by a strong permenant magnet and dried in a vacuum oven at 60 ℃

overnight. The separated MPs were weighed by an analytical balance with the precision of 0.005 mg after fully dried, and the recovery rate (η) was determined by eq1,

$$\eta = \frac{m}{M} \times 100\% \quad (1)$$

Where, η (%) is the recovery rate of MPs; m (mg) is the mass of separated MPs from suspension; M (mg) is the initial mass of MPs.

The adsorption capacity of NDs for 100 nm NPs was further studied. Specifically, 5 mg of NDs was added to varied concentrations of NP suspensions (10–150 mg L^{-1}), and a varied amount of NDs (0.5–10 mg) was used to absorb a constant 60 mg L^{-1} of NPs. The recovery rate (η) was determined by eq1.

2.5. PL analysis in MP separation

The variation of MP concentration in suspension before and after separation was measured by a PL spectrometer. The suspension through magnetic separation was measured at 470 nm of Ex and 620 nm of Em.

2.6. Adsorption of MP by NDs and separation mechanism

To investigate the impact on adsorption under different environmental factors, the separation experiments were carried out at different pH values (3–11) and temperatures (298 K, 308 K, and 318 K). For a series of batch adsorption experiments, 5 mg NDs as an adsorbent was added to 60 mg L^{-1} of NP suspension and incubated in an orbital shaker at 180 rpm for 0 to 180 min. The adsorption conditions were kept the same for real water experiments and the water environment is the seawater with a pH of 7.8.

The adsorption capacity (q_e) was determined by eq2, where c_0 and c_e (mg L^{-1}) are the concentration of MPs at the initial and equilibrium state; V (mL) is the MP suspension volume; m is the mass of adsorbent.

$$q_e = \frac{(c_0 - c_e)V}{m} \quad (2)$$

In addition, adsorption kinetics and isothermal models were applied to understand the interaction between NDs and MPs. The corresponding equations utilized for calculations are shown in Supporting Information.

2.7. Reusability of NDs on MP removal

Thermogravimetric analysis (TGA) was conducted by a simultaneous thermal analyser, from PerkinElmer, loading 5 mg of mixture containing the recovered NDs and MPs in an alumina crucible and heating it from 35 to 800 ℃ at 5 ℃/min under an N_2 atmosphere of 20 mL/min. The reusability of the prepared NDs was confirmed through repeated adsorption experiments for the same concentration of the MP suspension. The mixture of NDs and MPs after weighing was heated at 500 ℃ in tubular furnace for 2 h under N_2 atmosphere to remove MPs completely. The calcined NDs were added to 60 mg L^{-1} MP suspension, which was recycled 5 times, and the removal rate was determined by eq1.

3. Results and discussion

3.1. Characterization of NDs and MPs

The synthesis process of Fe_3O_4 NDs is schematically represented in Fig. 1. The morphological features of Fe_3O_4 NDs and MPs were examined by SEM. Fig. 2a shows the morphologies of the prepared Fe_3O_4 NDs. The Fe_3O_4 NDs exhibit an irregular decagon disk morphology, and the average diameter is approximately 451.1 nm (Figure S2a), which is exactly the same as that of Fe_2O_3 NDs (Figure S2b), proving that the morphology and structure are very stable even after high-temperature reduction. The high-resolution TEM and combined selected area with corresponding fast Fourier transform (FFT) images depicted in Fig. 2b and c offer a detailed representation of the sample's morphology and microstructure. As displayed in Fig. 2c, the ND with a selected area revealed lattice fringe spacings of 0.252 nm and 0.296 nm, corresponding to the (311) and (220) planes of cubic Fe_3O_4, respectively. The FFT pattern of the Fe_3O_4 NDs (insert Fig. 2c) exhibited distinct spots at 0.338 1/nm and 0.395 1/nm, which correlate to *d*-spacings of 0.296 nm and 0.253 nm, agreeing well with the planes of magnetite. Fig. 2d shows the XRD pattern of Fe_3O_4 NDs. The characteristic diffraction peaks at $2\theta = 30.12°$, 35.41°, 43.09°, 57.04°, and 62.62° can be well indexed to the (220), (311), (400), (511), and (440) spinel (JCPDS No.11–0614) structures of magnetite. The XRD crystal planes at higher angles align with the selected area FFT results from TEM, confirming the crystallographic orientation of the Fe_3O_4 NDs. In addition, the thickness of NDs was determined utilizing the AFM analysis, as illustrated in Figure S1. The measured thickness of a single ND is around 4.26 nm, which further confirms the ultra-thin nature of the Fe_3O_4 nanodisc.

The element composition of NDs was investigated using EDS analysis attached to the SEM. As shown in Figure S3, fabricated NDs are composed of only oxygen and iron with a ratio of 60.46 % and 39.54 % and EDS mapping (Figure S3c–e) also shows there is no aluminium ion residues. The chemical valance states of NDs are further analyzed using XPS. As shown in Figure S4a, the survey spectrum shows prominent peaks of Fe 2p and O 1 s respectively. The high-resolution Fe 2p spectrum can be deconvoluted into two primary peaks at 710.7 and 724.1 eV, which are attributed to the $2p_{3/2}$ and $2p_{1/2}$, and the small peaks at 718.6 and 732.9 eV represent the satellite peaks as shown in Figure S4b. The two peaks at binding energy of 712.1 and 726.7 eV correspond to the $2p_{3/2}$ and $2p_{1/2}$ of Fe^{3+}, and the two peaks centred at 710.6 and 723.2 eV could be attributed to the $2p_{3/2}$ and $2p_{1/2}$ of Fe^{2+}, indicating the formation of Fe_3O_4 phase in NDs., No peak of Al 2p from 71 to 80 eV is observed in Figure S4c. These results confirm that no metallic Al or Al_2O_3 was generated during the fabrication process, and they also indicate the successful transition from Fe_2O_3 to Fe_3O_4.

The magnetic properties of NDs were measured by using a SQUID magnetometer. Fig. 2e shows the hysteresis loop (at 300 K), indicating

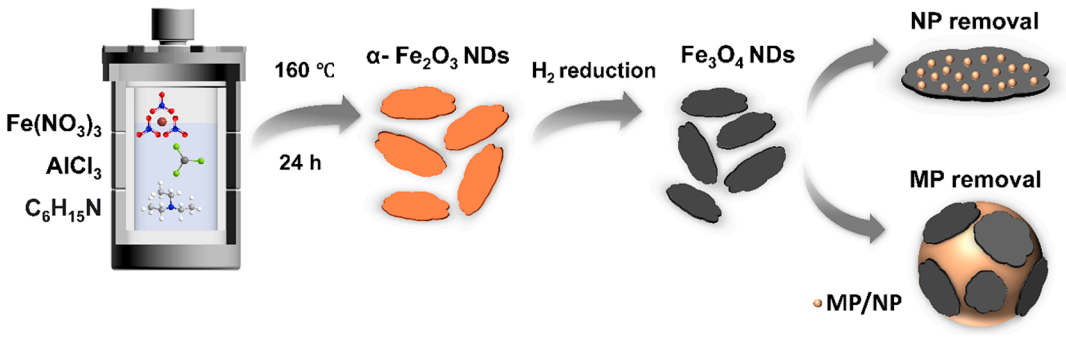

Fig. 1. Schematic representation of synthesis process on the formation of Fe_3O_4 NDs and MP adsorption process by NDs.

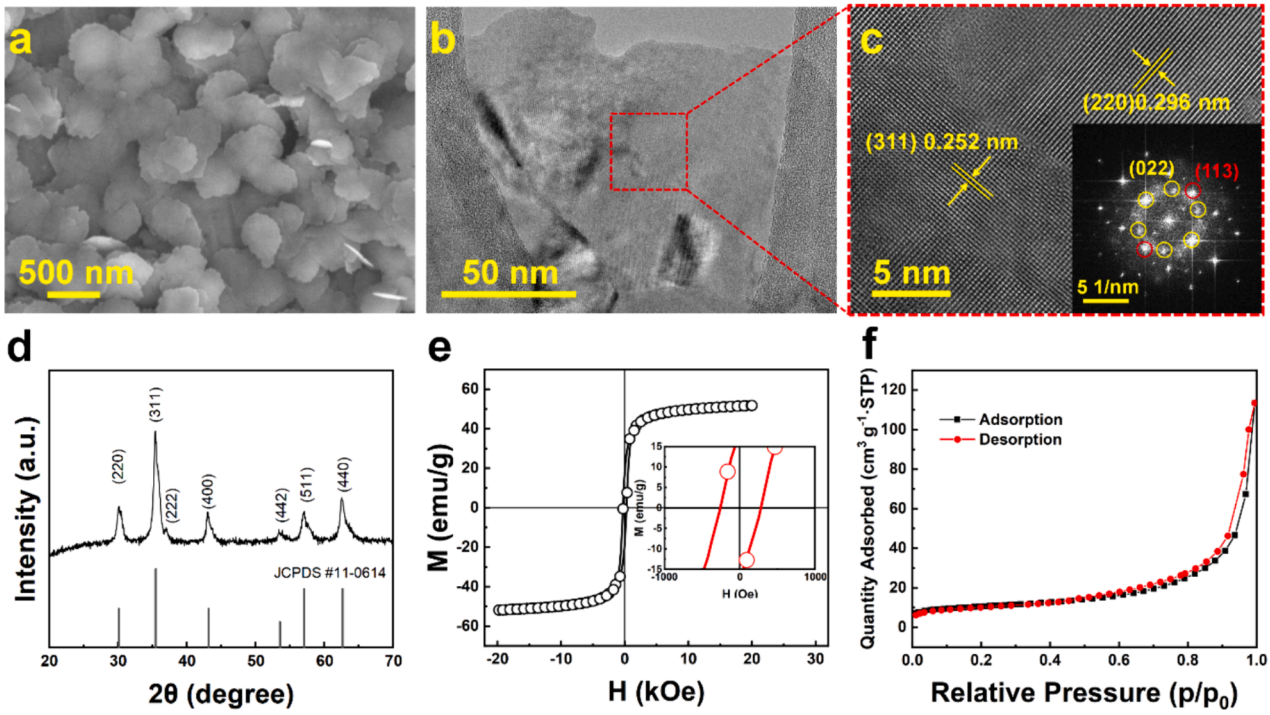

Fig. 2. (a) SEM images of Fe_3O_4 NDs; (b) TEM images of Fe_3O_4 NDs at relatively low amplification; (c) High resolution TEM images of a ND with FFT patterns (inset); (d) XRD patterns of Fe_3O_4 NDs. (e) Hysteresis loop of Fe_3O_4 ND. (f) N_2 adsorption–desorption isotherm of NDs at 300 K.

that the as-prepared Fe_3O_4 NDs exhibit soft magnetic behaviour with a relatively high saturation magnetization (56 emu/g) and low coercivity compared to Fe_3O_4 small nanoparticles [41,42]. The NDs specific surface area and porous nature were analyzed using the N_2 adsorption–desorption method. As shown in Fig. 2f, the sample displayed a type IV isotherm with a H4 hysteresis loop [28], indicative of mesoporous material characteristics and the presence of pore microstructures within the NDs. The specific surface area of NDs calculated using the BET is around 37.5 m^2 g^{-1}.

In this study, magnetic separation was conducted using seven types of microplastics (PE, PP, PA, PET, PVC, PMMA, and PS) with a size of 10 μm, NPs of PP, PE, PMMA, and PS with a size of 500 nm as well as PMMA and PS with a size of 100 nm. The MPs in 10 μm and 500 nm size were used to simply analyze removal capacity, while MPs in 100 nm size were used for both removal capacity and adsorption kinetics study. SEM and FTIR were carried out to confirm their sizes and polymer long-chain structures, as shown in Figure S5 and S6. It is to note that the actual sizes of PMMA are much smaller than the nominal sizes. Figure S7 shows the zeta potential of NDs at different pH values and Table S1 lists the zeta potential of the used MPs. It is observed that the surface charge of NDs exhibited a positive value in acidic conditions, while it is negative in basic conditions.

3.2. Separation of MPs

The microplastic in 10 μm and 500 nm were used to for the study of the removal capacity of NDs. As shown in Figure S8a, the removal efficiency of MP in 10 μm are 90 %, 93.5 %, 89.6 %, 87.4 %, 89.2 %, 93.1 %, and 75 % for PP, PET, PS, PE, PMMA, PVC, and PA respectively. Since the zeta potential of the PA suspension is significantly lower than that of other MP suspensions (Table S1), it is more prone to aggregation or sedimentation that results in a lower removal efficiency compared to other MPs. Fig. 3a and b are the SEM images of the separated PMMA and PS paricles with a size of 10 μm. It shows that NDs are well adsorbed on the MPs, which can enhance the separation efficiency when applying a magnetic field on these MPs. The SEM images of other MPs adsorbed by NDs are shown in Figure S8b–f. It can be seen that NDs fully cover the big microplastics, suggesting the well adsorption of MPs. Figure S9 shows the photographs of the microplastics in solution before and after separation. It is observed that the dispersion of MPs in water is different for seven types of MPs, resulting in differences in separation efficiency. NPs with a size of 500 nm (PS, PMMA, PE, PP) also underwent treatment with NDs. The separation efficiency and SEM images after separation are shown in Fig. 3c and d and Figure S10a and b. Due to the comparable size of NDs and MPs, the MPs directly attach on NDs. Some agglomerates are observed in the separated MPs, indicating the strong electrostatic force between MPs and NDs since the removal efficiency of MPs is still very high, which is 92.3 %, 94.3 %, 93.2 %, and 97 % for PMMA, PE, PS, PP, respectively, as shown in Figure S10c. When the MPs size are further reduced to around 100 nm, the small MPs will be adsorbed on NDs, as shown in Fig. 3e and f. It is seen that small NPs with a high density can be separated by the NDs, endorsing the high performance of NDs on the separation capacity of different sized MPs/NPs.

To further determine the adsorption capacity of NDs for 100 nm PS and PMMA, various concentrations (10–150 mg L^{-1}) of NPs were introduced to a constant quantity (5 mg) of NDs. Fig. 4a illustrates a gradual decrease in the removal efficiency of NPs with an increase in MP concentration. Once the concentration of NPs surpasses 120 mg L^{-1}, NPs tend to readily aggregate, leading to an abundance of nanoparticles in the system. This aggregation adversely affects the adsorption efficiency of magnetic adsorbents [28]. Thus, the optimal concentration of MPs for adsorption is 30–60 mg L^{-1} and hence we used various qualities of NDs, ranging from 0.5 to 10 mg, to separate 60 mg L^{-1} of MPs. Finally, the optimum removal efficiency was obtained when the mass of NDs was greater than 5 mg, as shown in Fig. 4b.

3.3. Adsorption kinetics

For a better understanding of the MP removal process by NDs, the adsorption kinetics were studied based on the effect of various contact time of NDs on PMMA and PS NPs at five pH values. The kinetic parameters and fitting curves are shown in Table S2, S3 and Fig. 4c and d.

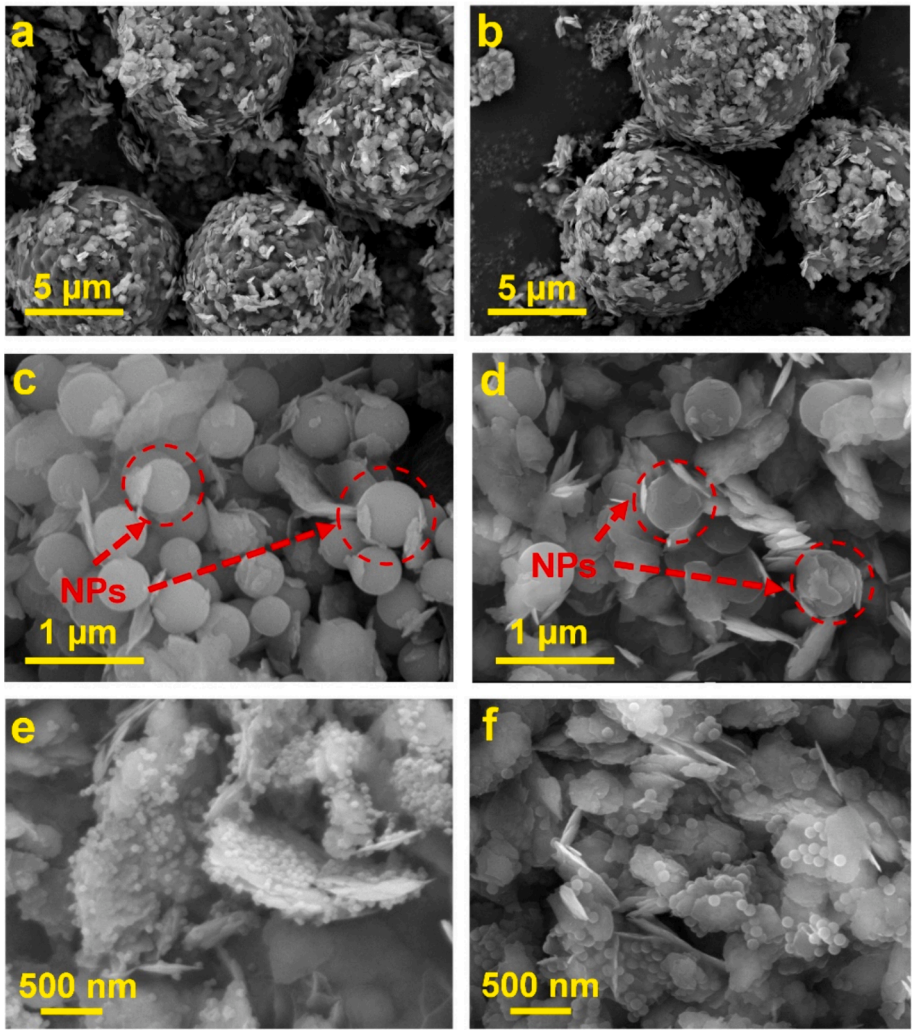

Fig. 3. SEM images of the separated 10 μm of PMMA (a); 10 μm of PS (b); 500 nm of PMMA (c); 500 nm of PS (d); 100 nm of PMMA (e); and 100 nm of PS (f).

The adsorption capacity of NDs rapidly increased in the first 10 min, reaching the maximum value and remaining equilibrium. The maximum adsorption capacity for PMMA at pH 3, 5, 7, 9, and 11 were 183.0, 183.2, 188.4, 101.1, and 70.2 mg g^{-1}, respectively. Similar adsorption results could also be obtained for PS, where the maximum adsorption capacity at pH 3, 5, 7, 9, and 11 were 174.7, 175.0, 187.7, 151.9, and 72.0 mg g^{-1}, respectively. It is obviously found that the adsorption capacity of NDs under acidic and neutral environments is significantly higher than that under basic environments. This confirmed that electrostatic attraction is the main driving force leading to NPs/MPs capture. In acidic and neutral environments, the zeta potential of the as-prepared NDs exhibited positive, while that of MPs was negative. The positive and negative difference in zeta potential contributed to the rapid adsorption in initial treatment and then effectively magnetized the MPs. Therefore, the pH of MP suspension plays an important role in MP removal, which has been extensively investigated in previous research associated with MP adsorption [28,32]. MP adsorption kinetics were analysed through fitting with non-linear kinetic models, including pseudo-first-order (PFO), pseudo-second-order (PSO), and intraparticle diffusion models, and their corresponding equations are listed in supporting information [28]. The adsorption kinetics of NPs with a size of 100 nm are more consistent with the PFO reaction under five different pH values, where all correlation coefficients(R^2) are greater than 0.97 and higher than that of the PSO model. It is worth noting that the adsorption at the beginning of the reaction was quite fast and the system could reach equilibrium within 30 min. This is attributed to the strong hydrophobic interaction between NDs and plastics, and an acidic or neutral environment can significantly intensify the electrostatic attraction between nanoparticles. However, a net repulsive effect will impede the MP adsorption with increased pH value [43]. In addition to PFO and PSO models, the intraparticle diffusion model was also applied to further understand MP adsorption kinetics. The intraparticle diffusion occurs in three stages, and the fitting curves and parameters are shown in Figure S11. This model assumes that the adsorbates diffuse to the porous surface and reach an adsorption equilibrium state. If the boundary layer thickness constants (C_i) are zero, the adsorption reaction rate is only subjected to be controlled by intraparticle diffusion. In this work, the adsorption process can also be regarded as three steps:(1) MPs rapidly move forward and adhere to the adsorbent surface due to surface charge differences. (2) MPs gradually occupy the adsorption points on adsorbents, and the adsorption rate was significantly reduced. (3) the adsorption process reached saturation, indicating the magnetization of MP is completed [28]. Although the slopes of fitting curves in different pH solutions exhibited $k_{i1} > k_{i2} > k_{i3}$, the values of C_{i1}, C_{i2}, and C_{i3} for each step are not zero. This means that intraparticle diffusion is not the only factor that governs the adsorption reaction of MPs [44]. Likewise, the value of R^2 significantly decreases in the last two steps, indicating intraparticle diffusion is not applicable after the adsorption occurs for 15–20 min.

FTIR and PL analysis were carried out to identify the changes before and after separation. Fig. 4e shows the FTIR spectra of pristine NDs and NDs after adsorbing two types of MPs on the surface. It is observed that

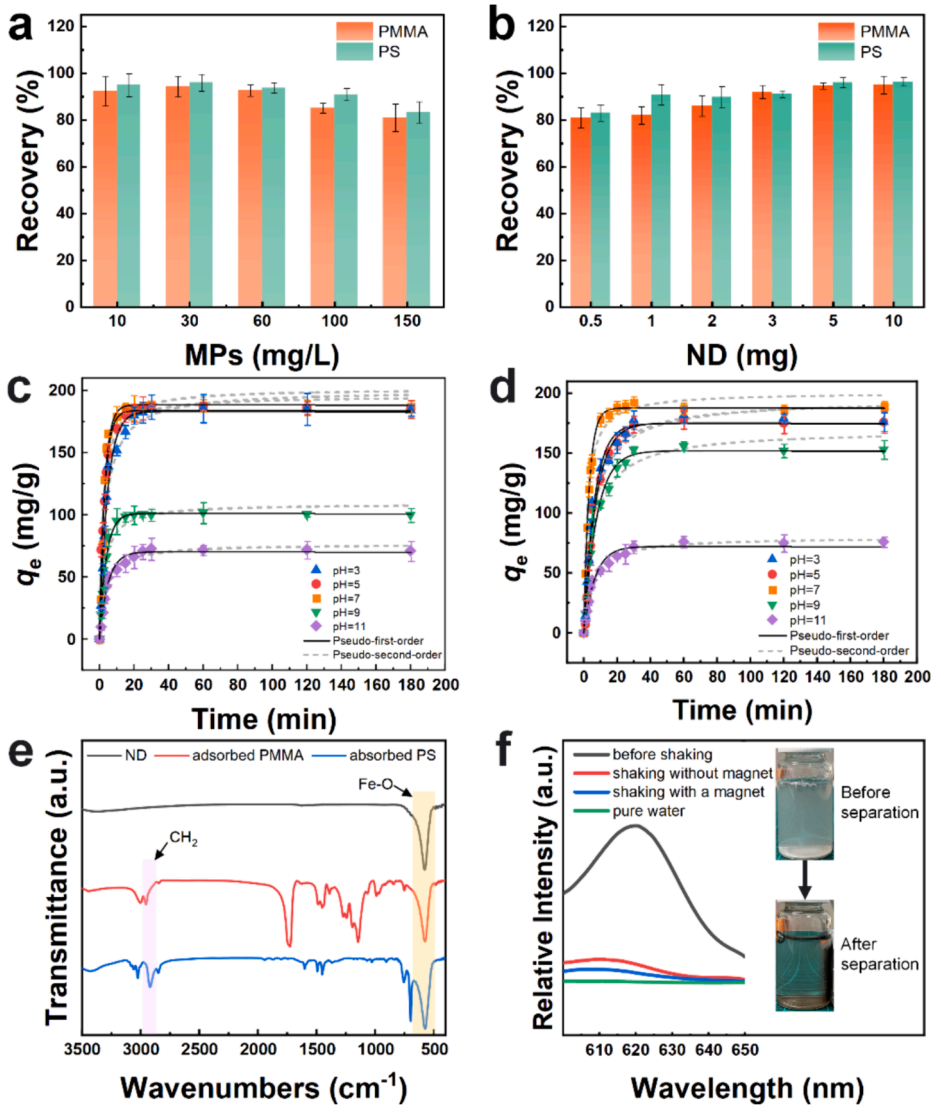

Fig. 4. (a) The removal efficiency of 100 nm PMMA and PS in various concentrations of MP suspensions; (b) The removal efficiency of 100 nm PMMA and PS by varying the mass of NDs; (c) Pseudo-first-order and pseudo-second order adsorption model of NDs for 100 nm of PMMA and (d) Pseudo-first-order and pseudo-second order adsorption model of NDs for 100 nm of PS; (e) FTIR spectra of NDs before and after adsorption; (f) PL spectra of NDs before and after adsorption.

there was not any peak corresponding to polymers for the pure NDs, but only Fe-O peak at 620 cm^{-1}. After adsorbing MPs, the intensity of characteristic peaks corresponding to polymer significantly increases, especially $–CH_2$ peak at 2916 cm^{-1}, indicating the adsorption of MPs. Likewise, the PL analysis was employed to further understand the capture of MPs with the magnetic NDs. The PL spectra of MP suspension with and without the adsorption of NDs are shown in Fig. 4f. Pure water exhibits no discernible characteristic peaks. However, water containing MPs manifests a prominent peak, indicative of the presence of MPs. Upon the introduction of NDs into the solution with agitation for 20 min, followed by removal using a permanent magnet, the characteristic peak intensity is significantly reduced, suggesting the effective capture of MPs by the NDs. To understand whether magnetic field can influence the capture of MPs, we applied a magnetic field during agitation stage. After the MPs in solution was collected by a permanent magnet, the characteristic peak of the solution in the PL spectrum is lower compared to solution without magnetic field during agitation. This observation implies that the application of a magnetic field may enhance the electrostatic adsorption force between NDs and MPs. This phenomenon may be due to the magnetizing of MPs during agitation state, which induces an extra attractive force between NDs and MPs. To the best of our knowledge, this particular phenomenon has not been previously reported, warranting further investigation to comprehensively understand the underlying mechanisms.

3.4. Adsorption isotherms

In the isothermal experiments, 5 mg of ND was used to adsorb different concentrations of 100 nm PMMA and PS (20–300 mg L^{-1}) in solution for 2 h at three different temperatures, i.e. 298 K, 308 K, and 318 K. The adsorption isotherms of NDs were analysed based on four adsorption isothermal models: Langmuir, Freundlich, Sips, and Temkin models, and their corresponding equations are shown in SI [28].The Langmuir and Freundlich isotherm models stand out as the two most commonly employed empirical models for analyzing the adsorption process. The Langmuir model describes the adsorption reaction is a monolayer homogeneous adsorption process and occurs on a uniform surface, while the Freundlich model assumes the adsorption is a multilayer adsorption process on an uneven surface [27,45]. The Sips isotherm model was derived from both the Langmuir and Freundlich isotherm models to describe the Freundlich multilayer adsorption at low adsorbate concentrations while predicting the monolayer adsorption

related to Langmuir at high concentrations [46]. In addition to the above three models, the Temkin model was also used to describe a linear decrease of adsorption energy in adsorption layers due to the interaction between adsorbents [47,48]. The corresponding parameters are shown and listed in Tables S4 and S5. From the fitting curves shown in Fig. 5, the adsorption capacity q_e was 216, 227, and 251 mg g^{-1} for PMMA and 234, 242, 257 mg g^{-1} at 298 K, 308 K, 318 K, respectively. At the elevated temperature, the adsorption capacity was slightly enhanced since extra thermal vibration energy was introduced and MPs diffusion was accelerated. The R^2 values of NDs for the Sips model were the highest among all isotherm models applied in this work. Therefore, the Sips isotherm model was the most appropriate empirical model to explain the MP adsorption by NDs. In Table S4, S5, 1/n represents the adsorption intensity, and its values are always less than 1, indicating the adsorption process of PMMA and PS by NDs is favourable and it is able to form strong electrostatic force between the adsorbent and MPs [27,49]. In addition, we compared the adsorption capacity of different magnetic adsorbents that were reported in the past three years, as listed in Table S6.

3.5. Adsorption mechanisms

The adsorption properties of MPs are strongly influenced by their surface characteristics, functional groups, crystallinity, structure and specific surface area. To understand the properties related to the adsorption capacity of MPs, the underlying adsorption mechanism is essential to be investigated. In this work, it is found that the size of NDs and MPs are crucial for the adsorption process, and when the size of MPs is 10 μm, which is greater than that of NDs, they act as the adsorbent. Conversely, when the size of plastic decreases to 100 nm, the NDs become the adsorbate, and while the MPs/NPs at an intermediate size of 500 nm, they are equally attached to the NDs. The hydrophobic properties of both MPs/NPs and NDs exhibited hydrophobic interactions, which lead to higher adsorption and this mechanism is often observed in the adsorption of organic pollutants onto carbon-based materials. Likewise, the Sips adsorption model indicates heterogeneous adsorption sites on the NDs due to the presence of different adsorption sites, which may have varying affinities for MPs/NPs, suggesting a complex adsorption process. The opposite zeta potentials of MPs/NPs and NDs facilitate strong electrostatic attraction because the particles with opposite charges attract each other [28,44,50]. To further understand the mechanisms of MP adsorption by NDs, we investigated the ground magnetization state of prepared NDs and the role of magnetism in MP separation. Unlike traditional superparamagnetic nanoparticles, NDs possess a vortex magnetic domain, allowing for good dispersion while maintaining ferromagnetic properties. On the other hand, magnetic nanoparticles with ultra-small sizes were usually used since they can adhere well to the MP surface. For those superparamagnetic nanoparticles, the magnetization of the materials is zero without applying an external magnetic field, therefore, the material cannot magnetize the MPs. Although the property allows magnetic nanoparticles to capture MPs when applying a magnetic field, the separation force is only contributed by the electrostatic [51–53]. Different from the above magnetic nanoparticles which were used in MPs separation, it has been proved that magnetic NDs have a vortex magnetic domain structure, where most spins exhibit a circular alignment in the plane of the ND [34,54], as shown in Fig. 6c. This kind of domain structure helps the well-dispersion of NDs in solution while maintaining the ferromagnetic state and relatively high saturation magnetization. The circular domain can trap the MPs/NPs on the surface of NDs, accelerating the separation process. During the agitation stage, an applied magnetic field will induce high magnetization of the NDs, leading to the magnetizing of MPs/NPs, further promoting the adsorption process. This unique magnetic nanodisc structure combined with the NDs large specific surface area enhanced the MP/NPs adsorption efficiency. From materials characterization, NDs also possess micropore strucuture, which make the adorsption mechanism complicated. The well-fitted Sips isotherm model in the adsorption represents the heterogeneous adsorption sites and

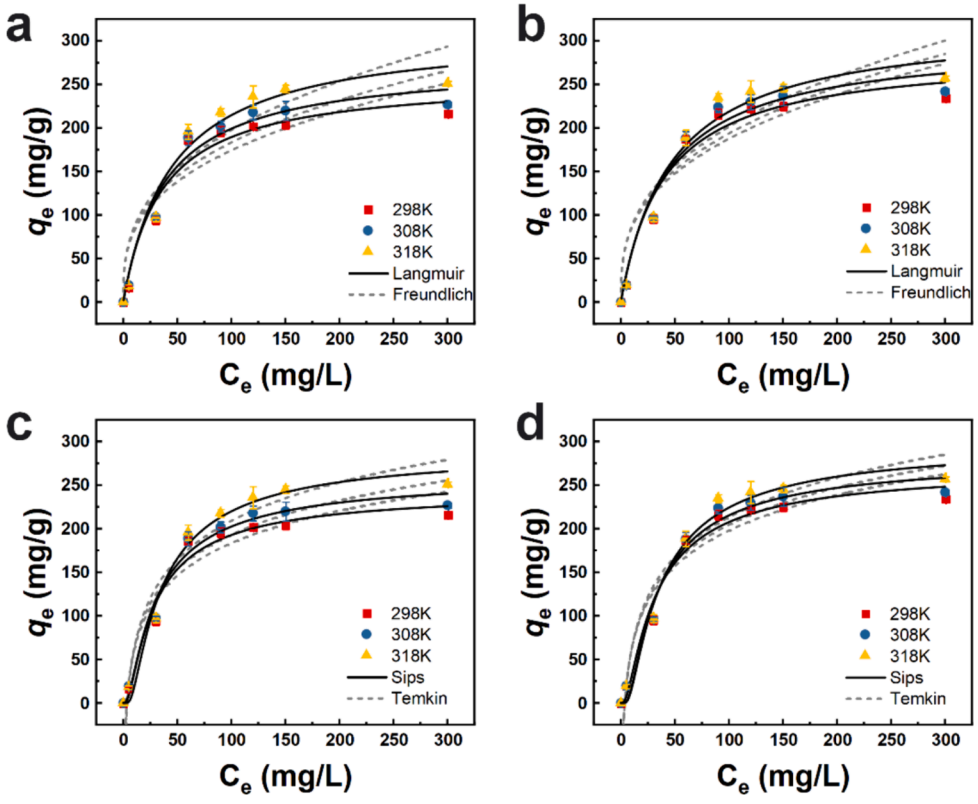

Fig. 5. Adsorption isotherm fitting of the NDs for the removal of 100 nm PMMA (a, c) and PS (b, d).

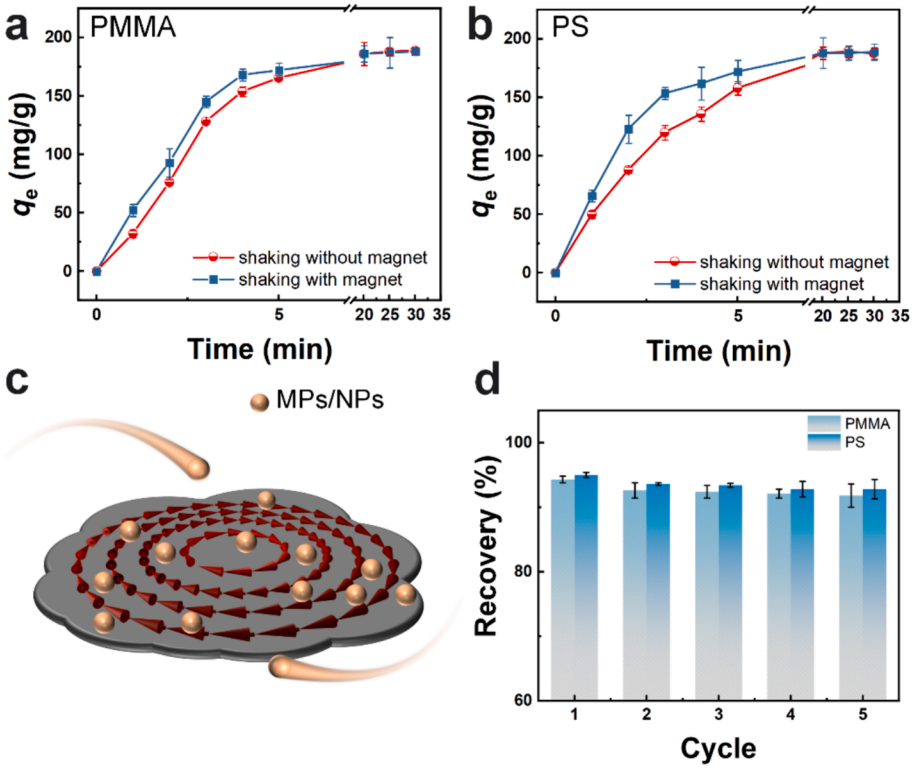

Fig. 6. The relationships between the adsorption capacity of NDs in seawater and time for 100 nm PMMA (a) and PS (b); (c) Magnetic vortex state in Fe_3O_4 NDs (d) The removal of efficiency of NDs over 5 cycles of NP separation.

complex adsorption mechanisms.

In addition, we conducted magnetic separation experiments in seawater, achieving high recovery rates for PMMA and PS NPs (Figure S12). We could notice that before separation the seawater contained a small amount of sand and added NPs (PMMA and PS) which were cleared after magnetic separation, leaving behind the heavy sand particles. As shown in Figure S13, the final recovery rate of 100 nm PMMA and PS reached 97.3 and 94.8 %, respectively. Moreover, experiments using PMMA and PS NPs in sea water were carried out to understand the influence of applied magnetic field during the adsorption process in addition to the adsorption kinetic studies (Fig. 6). From Fig. 6a and b we observed that the adsorption equilibrium time was shortened, and a higher adsorption capacity was achieved within the first 5 min when a magnetic field was applied during shaking. Applying a magnetic field during the adsorption process accelerated the rate of adsorption without affecting the maximum capacity observed. Therefore, the combination of vortex magnetic domain structure, large surface area and electrostatic attraction enables efficient and rapid magnetic separation of MPs and NPs using magnetic NDs.

3.6. Reusability of NDs on MP removal

In light of the regeneration of NDs, cost considerations, and the potential for large-scale applications, the reusability of NDs was assessed. The mixture of NDs and MPs were calcined at 500 ℃ under N_2 atmosphere, and the TGA analysis was carried out to confirm whether the plastics were completely removed at 500 ℃. The thermogram for the studied PMMA and PS, as shown in Figure S14, indicates that both PMMA and PS are fully decomposed at 500 ℃. Fig. 6d shows that the removal efficiency remains above 90 % even after MPs separation performed for five cycles. This indicates that the prepared NDs have promising stability after multiple adsorption and calcination steps. As a result, Fe_3O_4 NDs exhibit the capability for repetitive recycling while maintaining an excellent separation efficiency of MPs, promising for practical applications.

4. Conclusion

In this work, 2D ultrathin Fe_3O_4 NDs were fabricated to adsorb and separate MPs/NPs in an aquatic environment. The BET and magnetic study of NDs substantiated that magnetic nanomaterials characterized by a high specific surface area and a ground vortex magnetic state can effectively and efficiently remove both MPs and NPs. A comprehensive set of removal experiments was systematically conducted, encompassing MPs and NPs varied in size and category. For 10 μm MPs, the observed trend indicated that the removal rate was highest (93.5 %) for PET, whereas exhibited the lowest for PA (75 %). The removal rates for the remaining materials were maintained at approximately 90 %. For 500 nm NPs, the removal rates for the four types of NPs consistently exceeded 92 %, with PP exhibiting the highest removal rate at 97 %. Likewise, adsorption kinetics and isotherms of NDs for 100 nm of NPs were analyzed. It was found that the pH value has a pronounced impact on the adsorption capacity of NDs and the optimal adsorption capacity under a neutral condition could reach a value of 188.4 and 187.7 mg g^{-1} for PMMA and PS, respectively. Analyses of kinetics revealed the adsorption of NDs was relatively consistent with the PFO model. Four empirical adsorption isothermal models were also analyzed, and it was determined that the Sips isotherm model proved to be the most suitable empirical model for elucidating the adsorption of NPs by NDs. Furthermore, we identified that the process of adsorption and magnetizing by NDs was contributed from both electrostatic interaction and vortex magnetic domain. Finally, the prepared NDs demonstrated excellent reusability, sustaining a removal efficiency of over 90 % even after undergoing five cycles of separation. In this study, 2D magnetic nanomaterials were first used in MPs and NPs separation to obtain superior removal efficiencies. We also discovered that both the electrostatic interaction and special vortex magnetic state of NDs can lead to effective plastics adsorption from micro to nano, which offers a

reference for future magnetic separation methodology of plastic pollutants.

CRediT authorship contribution statement

Yitong Cao: Writing – original draft, Methodology, Investigation, Data curation. **C.I. Sathish:** Investigation, Methodology, Writing, Editing, Supervision. **Zhixuan Li:** Data curation. **Muhammad Ibrar Ahmed:** Data curation. **Vibin Perumalsamy:** Data curation. **Chaojie Cao:** Data curation. **Chenxi Yu:** Data curation. **Binodhya Wijerathne:** . **Adrew Fleming:** Data curation. **Liang Qiao:** Conceptualization. **Shaobin Wang:** Conceptualization. **Jiabao Yi:** Supervision, Methodology, Writing and Editing, Acquired Funding.

Declaration of competing interest

The authors declare that they have no known competing financial interests or personal relationships that could have appeared to influence the work reported in this paper.

Data availability

Data will be made available on request.

Acknowledgement

We acknowledge the financial support from Australian Research Council (LP210100436 and LP200201079).

Appendix A. Supplementary data

Supplementary data to this article can be found online at https://doi.org/10.1016/j.cej.2024.154610.

References

[1] Boucher, J.; Billard, G. The challenges of measuring plastic pollution. *Field Actions Science Reports. The Journal of Field Actions* 2019, (Special Issue 19), 68-75.
[2] R. Geyer, Production, use, and fate of synthetic polymers, Plastic Waste and Recycling. (2020) 13–32.
[3] R. Geyer, J.R. Jambeck, K.L. Law, Production, use, and fate of all plastics ever made, Sci. Adv. 3 (7) (2017) e17007782.
[4] A.L. Andrady, Plastics and environmental sustainability, John Wiley & Sons, 2015.
[5] M. Masry, S. Rossignol, J.L. Gardette, S. Therias, P.O. Bussiere, P. Wong-Wah-Chung, Characteristics, fate, and impact of marine plastic debris exposed to sunlight: A review, Mar. Pollut. Bull. 171 (2021) 112701, https://doi.org/10.1016/j.marpolbul.2021.112701.
[6] A. Cozar, F. Echevarria, J.I. Gonzalez-Gordillo, X. Irigoien, B. Ubeda, S. Hernandez-Leon, A.T. Palma, S. Navarro, J. Garcia-de-Lomas, A. Ruiz, et al., Plastic debris in the open ocean, PNAS 111 (28) (2014) 10239–10244, https://doi.org/10.1073/pnas.1314705111.
[7] R.C. Thompson, Y. Olsen, R.P. Mitchell, A. Davis, S.J. Rowland, A.W. John, D. McGonigle, A.E. Russell, Lost at sea: where is all the plastic? Science 304 (5672) (2004) 838–839.
[8] K.L. Law, R.C. Thompson, Oceans, Microplastics in the Seas. *Science* 345 (6193) (2014) 144–145, https://doi.org/10.1126/science.1254065.
[9] M. Zhang, Y. Zhao, X. Qin, W. Jia, L. Chai, M. Huang, Y. Huang, Microplastics from mulching film is a distinct habitat for bacteria in farmland soil, Sci. Total Environ. 688 (2019) 470–478, https://doi.org/10.1016/j.scitotenv.2019.06.108.
[10] S. Zhang, X. Yang, H. Gertsen, P. Peters, T. Salanki, V. Geissen, A simple method for the extraction and identification of light density microplastics from soil, Sci. Total Environ. 616–617 (2018) 1056–1065, https://doi.org/10.1016/j.scitotenv.2017.10.213.
[11] L. Yang, Y. Zhang, S. Kang, Z. Wang, C. Wu, Microplastics in freshwater sediment: A review on methods, occurrence, and sources, Sci. Total Environ. 754 (2021) 141948, https://doi.org/10.1016/j.scitotenv.2020.141948.
[12] A.A. Horton, C. Svendsen, R.J. Williams, D.J. Spurgeon, E. Lahive, Large microplastic particles in sediments of tributaries of the River Thames, UK - Abundance, sources and methods for effective quantification, Mar. Pollut. Bull. 114 (1) (2017) 218–226, https://doi.org/10.1016/j.marpolbul.2016.09.004.
[13] L. Nizzetto, G. Bussi, M.N. Futter, D. Butterfield, P.G. Whitehead, A theoretical assessment of microplastic transport in river catchments and their retention by soils and river sediments, Environ Sci Process Impacts 18 (8) (2016) 1050–1059, https://doi.org/10.1039/c6em00206d.
[14] D. Li, K. Liu, C. Li, G. Peng, A.L. Andrady, T. Wu, Z. Zhang, X. Wang, Z. Song, C. Zong, et al., Profiling the Vertical Transport of Microplastics in the West Pacific Ocean and the East Indian Ocean with a Novel in Situ Filtration Technique, Environ. Sci. Tech. 54 (20) (2020) 12979–12988, https://doi.org/10.1021/acs.est.0c02374.
[15] N.P. Ivleva, Chemical Analysis of Microplastics and Nanoplastics: Challenges, Advanced Methods, and Perspectives, Chem. Rev. 121 (19) (2021) 11886–11936, https://doi.org/10.1021/acs.chemrev.1c00178.
[16] C.M. Rochman, M.A. Browne, A.J. Underwood, J.A. van Franeker, R.C. T. Hompson, L.A. Amaral-Zettler, The ecological impacts of marine debris: unraveling the demonstrated evidence from what is perceived, Ecology 97 (2) (2016) 302–312, https://doi.org/10.1890/14-2070.1.
[17] K.L. Law, Plastics in the Marine Environment, Ann. Rev. Mar. Sci. 9 (2017) 205–229, https://doi.org/10.1146/annurev-marine-010816-060409.
[18] T.S. Galloway, M. Cole, C. Lewis, Interactions of microplastic debris throughout the marine ecosystem, Nat. Ecol. Evol. 1 (5) (2017) 116, https://doi.org/10.1038/s41559-017-0116.
[19] M. Smith, D.C. Love, C.M. Rochman, R.A. Neff, Microplastics in Seafood and the Implications for Human Health, Curr Environ Health Rep 5 (3) (2018) 375–386, https://doi.org/10.1007/s40572-018-0206-z.
[20] H.A. Leslie, M.J.M. van Velzen, S.H. Brandsma, A.D. Vethaak, J.J. Garcia-Vallejo, M.H. Lamoree, Discovery and quantification of plastic particle pollution in human blood, Environ. Int. 163 (2022) 107199, https://doi.org/10.1016/j.envint.2022.107199.
[21] K.L. Ng, J.P. Obbard, Prevalence of microplastics in Singapore's coastal marine environment, Mar. Pollut. Bull. 52 (7) (2006) 761–767, https://doi.org/10.1016/j.marpolbul.2005.11.017.
[22] H.K. Imhof, J. Schmid, R. Niessner, N.P. Ivleva, C. Laforsch, A novel, highly efficient method for the separation and quantification of plastic particles in sediments of aquatic environments, Limnol. Oceanogr. Methods 10 (7) (2012) 524–537, https://doi.org/10.4319/lom.2012.10.524.
[23] E.M. Crichton, M. Noel, E.A. Gies, P.S. Ross, A novel, density-independent and FTIR-compatible approach for the rapid extraction of microplastics from aquatic sediments, Anal Methods-Uk 9 (9) (2017) 1419–1428, https://doi.org/10.1039/c6ay02733d.
[24] J. Grbic, B. Nguyen, E. Guo, J.B. You, D. Sinton, C.M. Rochman, Magnetic Extraction of Microplastics from Environmental Samples, Environ Sci Tech Let 6 (2) (2019) 68-+, https://doi.org/10.1021/acs.estlett.8b00671.
[25] F. Rhein, F. Scholl, H. Nirschl, Magnetic seeded filtration for the separation of fine polymer particles from dilute suspensions: Microplastics, Chem. Eng. Sci. 207 (2019) 1278–1287, https://doi.org/10.1016/j.ces.2019.07.052.
[26] X. Shi, X. Zhang, W. Gao, Y. Zhang, D. He, Removal of microplastics from water by magnetic nano-Fe3O4, Sci. Total Environ. 802 (2022) 149838, https://doi.org/10.1016/j.scitotenv.2021.149838.
[27] H.-P. Wang, X.-H. Huang, J.-N. Chen, M. Dong, C.-Z. Nie, L. Qin, Modified superhydrophobic magnetic Fe3O4 nanoparticles for removal of microplastics in liquid foods, Chem. Eng. J. (2023) 476, https://doi.org/10.1016/j.cej.2023.146562.
[28] H. Zhao, X. Huang, L. Wang, X. Zhao, F. Yan, Y. Yang, G. Li, P. Gao, P. Ji, Removal of polystyrene nanoplastics from aqueous solutions using a novel magnetic material: Adsorbability, mechanism, and reusability, Chem. Eng. J. (2022) 430, https://doi.org/10.1016/j.cej.2021.133122.
[29] L. Wang, T. Liu, J. Xu, Z. Wang, Z. Lei, K. Shimizu, Z. Zhang, T. Yuan, Enhanced economic benefit of recycling Fe(3)O(4) for promotion of volatile fatty acids production in anaerobic fermentation of food waste, Bioresour. Technol. 369 (2023) 128428, https://doi.org/10.1016/j.biortech.2022.128428 From NLM Medline.
[30] K. Kang, Y. Hu, I. Khan, S. He, P. Fetahi, Recent advances in the synthesis and application of magnetic biochar for wastewater treatment, Bioresour. Technol. 390 (2023) 129786, https://doi.org/10.1016/j.biortech.2023.129786 From NLM Medline.
[31] N. Yan, B. Hu, Z. Zheng, H. Lu, J. Chen, X. Zhang, X. Jiang, Y. Wu, J. Dolfing, L. Xu, Twice-milled magnetic biochar: A recyclable material for efficient removal of methylene blue from wastewater, Bioresour. Technol. 372 (2023) 128663, https://doi.org/10.1016/j.biortech.2023.128663 From NLM Medline.
[32] N. Singh, N. Khandelwal, Z.A. Ganie, E. Tiwari, G.K. Darbha, Eco-friendly magnetic biochar: An effective trap for nanoplastics of varying surface functionality and size in the aqueous environment, Chem. Eng. J. (2021) 418, https://doi.org/10.1016/j.cej.2021.129405.
[33] J. Qu, M.S. Akindolie, Y. Feng, Z. Jiang, G. Zhang, Q. Jiang, F. Deng, B. Cao, Y. Zhang, One-pot hydrothermal synthesis of NaLa(CO3)2 decorated magnetic biochar for efficient phosphate removal from water: Kinetics, isotherms, thermodynamics, mechanisms and reusability exploration, Chem. Eng. J. (2020) 394, https://doi.org/10.1016/j.cej.2020.124915.
[34] D. Gregurec, A.W. Senko, A. Chuvilin, P.D. Reddy, A. Sankararaman, D. Rosenfeld, P.H. Chiang, F. Garcia, I. Tafel, G. Varnavides, et al., Magnetic Vortex Nanodiscs Enable Remote Magnetomechanical Neural Stimulation, ACS Nano 14 (7) (2020) 8036–8045, https://doi.org/10.1021/acsnano.0c00562.
[35] H.-M. Fan, M. Olivo, B. Shuter, J.-B. Yi, R. Bhuvaneswari, H.-R. Tan, G.-C. Xing, C.-T. Ng, L. Liu, S.S. Lucky, et al., Quantum Dot Capped Magnetite Nanorings as High Performance Nanoprobe for Multiphoton Fluorescence and Magnetic Resonance Imaging, J. Am. Chem. Soc. 132 (42) (2010) 14803–14811, https://doi.org/10.1021/ja103738t.
[36] H.-M. Fan, J.-B. Yi, Y. Yang, K.-W. Kho, H.-R. Tan, Z.-X. Shen, J. Ding, X.-W. Sun, M.C. Olivo, Y.-P. Feng, Single-Crystalline MFe2O4 Nanotubes/Nanorings

Synthesized by Thermal Transformation Process for Biological Applications, ACS Nano 3 (9) (2009) 2798–2808, https://doi.org/10.1021/nn9006797.
[37] Z. Nemati, S.M. Salili, J. Alonso, A. Ataie, R. Das, M.H. Phan, H. Srikanth, Superparamagnetic iron oxide nanodiscs for hyperthermia therapy: Does size matter? J. Alloy. Compd. 714 (2017) 709–714, https://doi.org/10.1016/j.jallcom.2017.04.211.
[38] H.N. Abdelhamid, H.F. Wu, Multifunctional graphene magnetic nanosheet decorated with chitosan for highly sensitive detection of pathogenic bacteria, J. Mater. Chem. B 1 (32) (2013) 3950–3961, https://doi.org/10.1039/c3tb20413h From NLM PubMed-not-MEDLINE.
[39] H. Teymourian, A. Salimi, S. Khezrian, Fe3O4 magnetic nanoparticles/reduced graphene oxide nanosheets as a novel electrochemical and bioeletrochemical sensing platform, Biosens. Bioelectron. 49 (2013) 1–8, https://doi.org/10.1016/j.bios.2013.04.034 From NLM Medline.
[40] Z. Li, Y. Sun, W. Huang, C. Xue, Y. Zhu, Q. Wang, D. Liu, Innovatively employing magnetic CuO nanosheet to activate peroxymonosulfate for the treatment of high-salinity organic wastewater, J. Environ. Sci. (china) 88 (2020) 46–58, https://doi.org/10.1016/j.jes.2019.07.011 From NLM Medline.
[41] H.-B. Xia, P. Foo, J. Yi, Water-Dispersible Spherically Hollow Clusters of Magnetic Nanoparticles, Chem. Mater. 21 (12) (2009) 2442–2451, https://doi.org/10.1021/cm900268z.
[42] H.-B. Xia, J. Yi, P.-S. Foo, B. Liu, Facile Fabrication of Water-Soluble Magnetic Nanoparticles and Their Spherical Aggregates, Chem. Mater. 19 (16) (2007) 4087–4091, https://doi.org/10.1021/cm070918q.
[43] G.A. Haghighat, S. Sadeghi, M.H. Saghi, S.K. Ghadiri, I. Anastopoulos, D. A. Giannakoudakis, J.C. Colmenares, M. Shams, Zeolitic imidazolate frameworks (ZIFs) of various morphologies against eriochrome black-T (EBT): Optimizing the key physicochemical features by process modeling, Colloids Surf A Physicochem Eng Asp (2020) 606, https://doi.org/10.1016/j.colsurfa.2020.125391.
[44] L. Fu, J. Li, G. Wang, Y. Luan, W. Dai, Adsorption behavior of organic pollutants on microplastics, Ecotoxicol. Environ. Saf. 217 (2021) 112207, https://doi.org/10.1016/j.ecoenv.2021.112207 From NLM Medline.
[45] H. Li, F. Wang, J. Li, S. Deng, S. Zhang, Adsorption of three pesticides on polyethylene microplastics in aqueous solutions: Kinetics, isotherms, thermodynamics, and molecular dynamics simulation, Chemosphere 264 (Pt 2) (2021) 128556, https://doi.org/10.1016/j.chemosphere.2020.128556 From NLM Medline.
[46] N. Tzabar, H.J.M. ter Brake, Adsorption isotherms and Sips models of nitrogen, methane, ethane, and propane on commercial activated carbons and polyvinylidene chloride, Adsorption 22 (7) (2016) 901–914, https://doi.org/10.1007/s10450-016-9794-9.
[47] X. Chen, X. Gu, L. Bao, S. Ma, Y. Mu, Comparison of adsorption and desorption of triclosan between microplastics and soil particles, Chemosphere 263 (2021) 127947, https://doi.org/10.1016/j.chemosphere.2020.127947 From NLM Medline.
[48] Y. Leng, W. Wang, H. Cai, F. Chang, W. Xiong, J. Wang, Sorption kinetics, isotherms and molecular dynamics simulation of 17beta-estradiol onto microplastics, Sci. Total Environ. 858 (Pt 3) (2023) 159803, https://doi.org/10.1016/j.scitotenv.2022.159803 From NLM Medline.
[49] N.T.R.N. Kumara, N. Hamdan, M.I. Petra, K.U. Tennakoon, P. Ekanayake, Equilibrium Isotherm Studies of Adsorption of Pigments Extracted from Kudukkuduk (Melastoma malabathricumL.) Pulp onto TiO2Nanoparticles, J. Chem. (2014,) 1–6, https://doi.org/10.1155/2014/468975.
[50] R. Kumar, A. Verma, M.R.J. Rakib, P.K. Gupta, P. Sharma, A. Garg, P. Girard, T. M. Aminabhavi, Adsorptive behavior of micro(nano)plastics through biochar: Co-existence, consequences, and challenges in contaminated ecosystems, Sci. Total Environ. 856 (Pt 1) (2023) 159097, https://doi.org/10.1016/j.scitotenv.2022.159097 From NLM Medline.
[51] T. Vangijzegem, V. Lecomte, I. Ternad, L. Van Leuven, R.N. Muller, D. Stanicki, S. Laurent, Superparamagnetic Iron Oxide Nanoparticles (SPION): From Fundamentals to State-of-the-Art Innovative Applications for Cancer Therapy, Pharmaceutics 15 (1) (2023), https://doi.org/10.3390/pharmaceutics15010236.
[52] O. Petracic, Superparamagnetic nanoparticle ensembles, Superlattice. Microst. 47 (5) (2010) 569–578, https://doi.org/10.1016/j.spmi.2010.01.009.
[53] Y. Cao, C.I. Sathish, X. Guan, S. Wang, T. Palanisami, A. Vinu, J. Yi, Advances in magnetic materials for microplastic separation and degradation, J. Hazard. Mater. 461 (2024) 132537, https://doi.org/10.1016/j.jhazmat.2023.132537.
[54] Y. Yang, X. Liu, Y. Lv, T.S. Herng, X. Xu, W. Xia, T. Zhang, J. Fang, W. Xiao, J. Ding, Orientation Mediated Enhancement on Magnetic Hyperthermia of Fe3O4 Nanodisc, Adv. Funct. Mater. 25 (5) (2014) 812–820, https://doi.org/10.1002/adfm.201402764.